The distribution of mutual inclinations arising from the stellar quadrupole moment

Kathleen Schultz [ID],[1]⋆ Christopher Spalding [ID][2,3]† and Konstantin Batygin[4]

[1]*Department of Physics and Astronomy, University of Maine, Orono, ME 04469, USA*
[2]*Department of Astrophysical Sciences, Princeton University, Princeton, NJ 08540, USA*
[3]*Department of Astronomy, Yale University, New Haven, CT 06511, USA*
[4]*Division of Geological and Planetary Sciences, Caltech, Pasadena, CA 91125, USA*

ABSTRACT

A large proportion of transiting planetary systems appear to possess only a single planet as opposed to multiple transiting planets. This excess of singles is indicative of significant mutual inclinations existing within a large number of planetary systems, but the origin of these misalignments is unclear. Moreover, recent observational characterization reveals that mutual inclinations tend to increase with proximity to the host star. These trends are both consistent with the dynamical influence of a strong quadrupolar potential arising from the host star during its early phase of rapid rotation, coupled with a non-zero stellar obliquity. Here, we simulate a population of planetary systems subject to the secular perturbation arising from a tilted, oblate host star as it contracts and spins down subsequent to planet formation. We demonstrate that this mechanism can reproduce the general increase in planet–planet mutual inclinations with proximity to the host star, and delineate a parameter space wherein the host star can drive dynamical instabilities. We suggest that approximately 5–10 per cent of low-mass *Kepler* systems are susceptible to this instability mechanism, suggesting that a significant number of single-transiting planets may truly be intrinsically single. We also report a novel connection between instability and stellar obliquity reduction and make predictions that can be tested within upcoming *TESS* observations.

Key words: planets and satellites: dynamical evolution and stability – planets and satellites: formation – planet–star interactions – stars: rotation.

1 INTRODUCTION

Our Solar system consists of eight planets, orbiting the Sun within a few degrees of a common plane. This coplanar architecture stood as a primary motivation for the development of the 'nebular hypothesis' (Kant 1755; Laplace 1796) – the notion that planetary systems form in a low aspect-ratio disc of dust and gas. A natural expectation is that extrasolar planetary systems share this coplanar architecture.

Individual extrasolar planetary inclinations are often difficult to measure (Fabrycky et al. 2014; Winn & Fabrycky 2015). Nevertheless, at a population level, lower mutual inclinations typically result in a larger number of planets observed to transit any given star (Ragozzine & Holman 2010; Lissauer et al. 2011; He, Ford & Ragozzine 2019). To that end, observational surveys have repeatedly found an excess of systems containing only one transiting planet, relative to that which would be expected if extrasolar planetary systems typically possessed a Solar system-like, coplanar arrangement (known as the 'Kepler Dichotomy'; Johansen et al. 2012; Ballard & Johnson 2016; Zhu et al. 2018). Henceforward in this work, we will refer to systems with a lone transiting planet as 'single-transiting

systems', and to the observed planet in question as a 'single-transiting planet', with similar terms for systems with multiple transiting planets.

An excess of single-transiting systems suggests one of two physical scenarios (Lissauer et al. 2011; Johansen et al. 2012; Ballard & Johnson 2016). First, perhaps these single-transiting planets are truly single, that is, they exist in systems lacking undiscovered non-transiting companions. Alternatively, the excess of singles might suggest that a substantial fraction of planetary systems possess multiple planets, but these planets' orbits are often inclined with one another by more than a few degrees (Johansen et al. 2012; Sanchis-Ojeda et al. 2014; Adams et al. 2020). To overcome this degeneracy, a combination of statistical analyses (He et al. 2019) and searches for signs of transit-timing variations (Zhu et al. 2018) have been performed. These efforts imply that the excess of singles emerges predominantly by way of large mutual inclinations within higher multiplicity systems. However, it is difficult to constrain the exact fraction of systems that are truly single, which have been suggested to constitute roughly 10 per cent of single-transiting planets (He et al. 2020).

Given the expected coplanarity of protoplanetary discs, the widespread existence of mutual inclinations among planetary systems requires a physical explanation. Hypotheses involving planet–planet scattering require planets of excessively large mass (Johansen et al. 2012), and self-excitation appears insufficient (Becker &

⋆ E-mail: kathleen.schultz@maine.edu
† 51 Pegasi b Fellow.

Adams 2016). The presence of an inclined exterior giant is capable of misaligning close-in planets (Becker & Adams 2017; Hansen 2017; Lai & Pu 2017), but requires that the giant obtained a mutual inclination in the first place (Pu & Lai 2020). While ∼30 per cent of close-in systems of super-Earths possess exterior giants (Bryan et al. 2019), their orbits tend to be aligned with inner groups of multiple transiting planets (Masuda, Winn & Kawahara 2020), but are poorly constrained around apparently-single transiting planets.

An additional source of dynamical heating may arise from the host star itself (Spalding & Batygin 2016). Specifically, while young, Sun-like stars spin relatively fast, acquiring a substantial quadrupole moment (Kraft 1967; Ward, Colombo & Franklin 1976). In concert, observational characterization of the spin vectors of planet-hosting stars indicate that substantial values of stellar obliquity, the angle between the stellar spin pole and the planet orbit, are widespread (Winn et al. 2010; Albrecht et al. 2012; Winn & Fabrycky 2015; Winn et al. 2017). Their origins remain uncertain, but viable pathways exist toward misalignments arising within the earliest 10–100 Myr in many cases (Batygin 2012; Spalding & Batygin 2014; Davies 2019). Thus, a significant fraction of planetary systems likely experienced an early epoch during which they felt the gravitational influence of a rapidly-rotating, tilted star.

The quadrupole moment of the central star tends to drive precession of the longitudes of ascending node among close-in planets (Murray & Dermott 1999). Shorter-period planets precess faster, thereby misaligning the orbits of close-in planets within a given system owing to differential precession about the star's inclined spin pole. This mechanism has been shown to lead to misalignments (Spalding & Batygin 2016), but also to dynamical instability for sufficiently inclined and oblate stars (Spalding, Marx & Batygin 2018).

A prediction of the oblate, tilted star (or 'OTS') mechanism is that planets residing closer to the host star are expected to exhibit larger mutual inclinations (Spalding & Batygin 2016). Such a trend has emerged from recent characterization of multitransiting planetary systems (Dai, Masuda & Winn 2018). Specifically, planets residing closer than ∼5 stellar radii exhibit larger mutual inclinations than more distant orbits. Many of these planets fall into the category of ultrashort period planets (USPs), which have orbital periods shorter than ∼1 d (Winn, Sanchis-Ojeda & Rappaport 2018). Among this population, almost all are expected to possess exterior planets within 50 d (Sanchis-Ojeda et al. 2014; Adams et al. 2020), further suggesting that the observed excess of single-transiting planets is primarily indicative of mutual inclinations.

A direct application of the OTS mechanism, as described here, has successfully reproduced the observed mutual inclinations among USPs theoretically (Li, Dai & Becker 2020). This work suggests that the trend observed by Dai et al. (2018) is consistent with forcing from an oblate host star, at least in the case of static stellar oblateness. However, the stellar quadrupole moment falls substantially with time as the star spins down and contracts on the pre-main sequence (Bouvier et al. 2014). The resulting sweeping of secular resonances is important for the excitation of mutual inclinations among the planetary orbits (Ward 1981; Spalding et al. 2018). Moreover, if the star possesses obliquities beyond ∼30°, the stellar contraction may excite dynamical instabilities (Spalding et al. 2018). It is thus important to deduce the fraction of systems, including those hosting USPs, expected to undergo instabilities due to the perturbations from a contracting host star, which is the focus of the present study.

In this work, we simulate a range of fabricated planetary systems. We inform our simulations using empirical constraints upon the typical masses and orbital separations within the *Kepler* data set

(Millholland, Wang & Laughlin 2017; Weiss et al. 2018). From these simulations, we obtain a relationship between the planetary orbital properties and the systems' eventual mutual inclinations. Consistently with Li et al. (2020), we reproduce the trend seen in Dai et al. (2018); however, we identify a significant population of systems that undergo dynamical instability, leaving behind only a single planet. Though this population of intrinsic singles may be rarer, they provide additional observational tests of the OTS mechanism, which we describe.

The remainder of this paper is organized as follows. In Section 2, we describe the set-up of our *N*-body experiments, with the results presented in Section 3. In Section 4, we discuss the requirements for and implications of instability, and assess the influence that various early-stage processes may have on the initial assumptions we have made in our model. We conclude in Section 5 with predictions and notes for future work.

2 METHODS

Our objective is to simulate the time evolution of the angle between two planets' orbital planes in a variety of *Kepler*-like two-planet systems. We suppose that initially, there exists a non-zero misalignment between the plane of the orbits and the stellar equator. The young host star possesses an appreciable quadrupole moment due to its own rapid rotation immediately following disc-dispersal (Bouvier et al. 2014). Over the subsequent hundreds of millions of years, the rotation rate slows owing to magnetic braking from stellar winds (Kraft 1967). To incorporate planet-planet interactions in addition to the decaying stellar quadrupole, we perform *N*-body simulations using the software package MERCURY6(Chambers 1999), employing the hybrid Bulirsch–Stoer/symplectic algorithm.

2.1 Model set-up

The gravitational potential of the central star was modelled up to quadrupole order (Murray & Dermott 1999). Moreover, general relativistic apsidal precession was modelled by way of the addition of a dipole-like potential as described in Nobili & Roxburgh (1986) (see their equation 10). Once both of these effects are included within the simulation via a user-defined subroutine, the stellar potential in spherical coordinates is given by

$$V_\star(t) = -\frac{GM_\star}{r}\left[1 + 3\frac{GM_\star}{rc^2} - \frac{3}{2}J_2(t)\left(\frac{R_\star}{r}\right)^2 \mathcal{P}_2(\cos(\theta))\right], \quad (1)$$

where the second gravitational harmonic J_2 is explicitly time-dependent and $\mathcal{P}_2$ is the second-degree Legendre polynomial. We define the stellar mass and radius as $M_\star$ and $R_\star$, while G is Newton's gravitational constant and c is the speed of light. The star's orientation is held fixed, and so θ is measured from the the stellar spin axis, while r is the radial distance from the stellar centre.

The magnitude of J_2 was forced to decay exponentially with time, from an initial value of $J_{2,0}$, over a time-scale $\tau_\star$:

$$J_2(t) = J_{2,0}\exp\left(-\frac{t}{\tau_\star}\right). \quad (2)$$

While this expression may not exactly reflect the time-evolution of a star's J_2, the decay occurs on a time-scale far exceeding the secular time-scales of the orbits. Thus, the evolution is adiabatic and so the exact time-dependence of J_2 is unimportant (Henrard 1982; Morbidelli 2002). In addition, as can be seen from equation (1), the dynamically-important quantity with respect to the stellar quadrupolar potential is not J_2 but $J_2R_\star^2$. The stellar radius contracts by over

a factor of 2 during the pre-main sequence, leading to a factor of 4 change in $J_2 R_\star^2$. For computational convenience, we encode all time-dependence within J_2 and hold $R_\star$ fixed at $R_\star = R_\odot$. This assumption slightly underestimates the quadrupolar potential at the earliest times. Nevertheless, Solar-type stars have undergone the majority of their contraction by the time the protoplanetary disc disperses (Gregory, Adams & Davies 2016), such that the effect of contraction should be of order unity.

The time step of our numerical simulations was set at 0.05 times the shortest planetary period, such that energy in the system at each step is conserved to within approximately $\sim 10^{-6}$ of its initial value.

2.2 Initial conditions

Our modelling seeks to deduce the importance of stellar obliquity and oblateness (parameterized through J_2) upon the orbital evolution of two-planet systems. As mentioned above, we assume that the stellar spin-axis is held fixed, an assumption that stems from the much greater angular momentum of the star as compared with the planetary systems considered here (Spalding et al. 2018), as well as from the additional assumption that any distant objects excluded from the model exert negligible perturbations upon the star and system. For simplicity, we fix the star's spin axis as along the z-axis. Both planetary orbital planes are initially aligned with one another, and the orbits are circular. Stellar obliquity is defined as the angle between the host star's spin angular momentum vector and the angular momentum vector of the planets' coplanar orbits; it is geometrically equivalent to the angle between those orbits and the host's equatorial plane. Given our assumption of a z-axis-aligned stellar spin pole, the initial stellar obliquity is equivalent to the planetary orbital inclination angle.[1] Thus, we parametrize stellar obliquity, represented as $\beta_\star$, in the form of non-zero initial orbital inclinations in our simulations.

Each system is constructed using a unique combination of stellar obliquity $\beta_\star$, initial stellar oblateness $J_{2,0}$, the innermost planet's semimajor axis a_1, and the planet mass m. The range of a_1 was selected to complement empirical data gathered by Dai et al. (2018). We choose to simulate 15 cases, given by

$$a_1/R_\star \in \{2, 3, 4, 5, 6, 7, 8, 9, 10, 11, 12, 14, 16, 18, 20\}. \quad (3)$$

These parameters are typical for the observed range of *Kepler* systems (Akeson et al. 2013). For simplicity, the host stars in our simulations are all of mass $1\,M_\odot$ and radius $1\,R_\odot = 0.005$ AU. Accordingly, the initial separations between host and nearest orbiting planet span between 0.01 and 0.1 AU.

Statistical evaluation of *Kepler* data has found that planets in two-planet systems tend to be separated by about 20 mutual Hill radii on average (Weiss et al. 2018). The mutual Hill radius R_H between planets j and $j+1$ is defined as (Gladman 1993)

$$R_H = \left(\frac{m_j + m_{j+1}}{3 M_\star}\right)^{1/3} \left(\frac{a_j + a_{j+1}}{2}\right), \quad (4)$$

for semimajor axes a_j, planetary masses m_j, and stellar mass M_*. In our simulations, we fix planet–planet separation at 20 Hill radii (Weiss et al. 2018), such that

$$a_{j+1} - a_j = 20 R_H. \quad (5)$$

---

[1]Note that stellar obliquity, in its most general case, is different for each orbit. Only by initializing the two planets to share the same orbital inclination, is it possible to define a single stellar obliquity in a two-planet system.

We parametrize our simulations in terms of a_1, the inner planet's semimajor axis, and set the two masses equal to one another. Thus, the value of a_2 is computed from a_1 as

$$a_2 = a_1 \left(\frac{1 - 10\mu^{1/3}}{1 + 10\mu^{1/3}}\right), \quad (6)$$

where we define $\mu \equiv 2m_1/3M_\star$.

Within a given *Kepler* system, planets tend to be more similar to one another in both radius (Weiss et al. 2018) and mass (Millholland et al. 2017) than would be expected if they had been randomly assigned from the entire *Kepler* catalogue. Critically for numerical simulations, this uniformity in mass allows us to select a single mass value m and assign it to both planets in a simulated system. According to Weiss & Marcy (2014), Keplerian sub-Neptunes have a mean mass of about 4.3 Earth masses; we have therefore selected planet masses of 1, 5, and 10 $M_\oplus$ in this work. However, we later find that planetary mass makes little difference to our conclusions.

A system is determined to have gone unstable when it loses one of its planets, either by ejection from the system or by collision with the host star. Previous investigations of the OTS mechanism have suggested that instability may occur in systems with stellar obliquities at or above about 30° (Spalding & Batygin 2016; Spalding et al. 2018). Here, we seek to explore the expected properties both of systems that remain stable, and of those that undergo instability. Accordingly, we chose a distribution of obliquities spanning the ranges above and below the expected instability limit, with more resolution below 30°:

$$\beta_* \in \{1, 6, 10, 20, 30, 50, 70\}^\circ. \quad (7)$$

To first order in stellar spin rate $\Omega_\star$, the magnitude of J_2 at the beginning of integration may be related to the stellar Love number k_2, mass and radius through the approximate expression (Sterne 1939; Ward et al. 1976; Spalding & Batygin 2016)

$$J_{2,0} \approx \frac{1}{3} k_2 \left(\frac{\Omega_\star^2}{G M_\star/R_\star^3}\right). \quad (8)$$

The quantity $G M_\star/R_\star^3$ above may be identified as the square of the stellar break-up spin frequency.

The Love number, k_2, for a young star can vary by an order of magnitude depending upon whether the star is assumed as fully convective or fully radiative (e.g. Batygin & Adams 2013, Sterne (1939)). At the beginning of our simulations, the star is yet to reach the main sequence, and is therefore likely to be fully convective, such that we assume an appropriate value of $k_2 = 0.28$. Note that lower mass stars leave the main sequence later than higher mass stars (Gregory et al. 2016). Thus, k_2 may change from system to system, which constitutes an important area of follow-up in order to predict dependencies between mutual inclinations and stellar type.

Observations constrain the spin periods of young stars to between 1 and 10 d (Bouvier et al. 2014). Given these empirical constraints, we created an initial set of $J_{2,0}$ based on ten spin periods evenly distributed in log space within the 1–10 d range. We also selected an additional five $J_{2,0}$ to explore the parameter space above $\sim 10^{-3}$; the proposed oblateness boundary between stability and instability in Spalding et al. (2018). The entire set of initial $J_{2,0}$ inputs in log space is

$$\begin{aligned} \log_{10}(J_{2,0}) \in \{ &-4.7, -4.5, -4.3, -4.1, -3.9, \\ &-3.7, -3.5, -3.3, -3.1, -2.9, \\ &-2.7, -2.5, -2.3, -2.1, -1.9\}. \quad (9) \end{aligned}$$
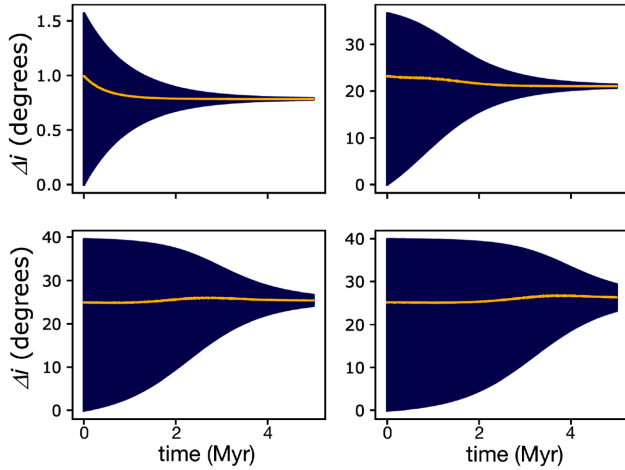
Figure 1. Four examples of mutual inclination (Δi) evolution when two planets are integrated for 5 Myr around a tilted star with decaying oblateness, for different initial strengths of quadrupole moment. Each planet pair in this subset is identical, with $a_1/R_* = 6$ and an average planet mass of 5 $M_\oplus$. Stellar obliquity is fixed at $20°$ in all four cases. From the left- to right-hand side, top to bottom, the systems were initialized with $J_{2,0}$ values of 1.98×10^{-5}, 7.89×10^{-4}, 3.14×10^{-3}, and 7.89×10^{-3}, respectively. The gold curves denote mean Δi averaged across 10-kyr intervals.

The full set of simulations is thus comprised of 4725 planetary systems, each representing a unique combination of the four system parameters a_1, m, β_*, and $J_{2,0}$. As described above, J_2 decays on a time-scale τ_*. In reality, stars spin-down over time-scales of 0.1–1 Gyr (Bouvier et al. 2014). However, for the purposes of our simulations, we can adopt any value that's much longer than the planets' forced precession frequencies (Henrard 1982; Morbidelli 2002). We set the decay time-scale to be $\tau_* = 1$ Myr, and ran the simulations for 5 Myr, or until only one planet remained. This simulation duration was sufficient to allow the stellar quadrupole moment to weaken such that mutual inclinations between planets in surviving systems settled into steady oscillations (see Fig. 1). A single mutual inclination (denoted by Δi) value is reported for each system that remained stable. We compute Δi by averaging the mutual planet–planet inclinations over the last 10 000 yr of the simulation.

2.3 Empirical parameter distributions

The data resulting from our suite of simulations provides a grainy, 4-dimensional grid that relates mutual inclination to β_*, $J_{2,0}$, m, and a_1. Our goal is to use these relationships to construct a predicted distribution of mutual inclinations resulting from the observed set of these four parameters. To do this, we must first fit a continuous function that relates Δi to $J_{2,0}$ and β_* for any given m and a_1. Next, we draw from empirically informed distributions of $J_{2,0}$ and β_* in order to construct a predicted Δi for each a_1 and m, marginalized over the stellar spin and tilt.

Both a_1 and m were drawn from uniform distributions, on [0.01, 0.1] AU and [1,10] $M_\oplus$, respectively. Observations of stellar mass and radius (Briceño et al. 2005) and spin rate (Karim et al. 2016) in the Orion OB1 association allow us to estimate J_2 for a real population of young, rapidly rotating stars. Specifically, we compiled a list of stars that appear in both databases from Briceño et al. (2005) and Karim et al. (2016), then calculated each star's J_2 using equation (8). The best-fitting distribution to the resulting J_2 set is illustrated in the upper panel of Fig. 2. Our 'artificial' $J_{2,0}$ values were drawn
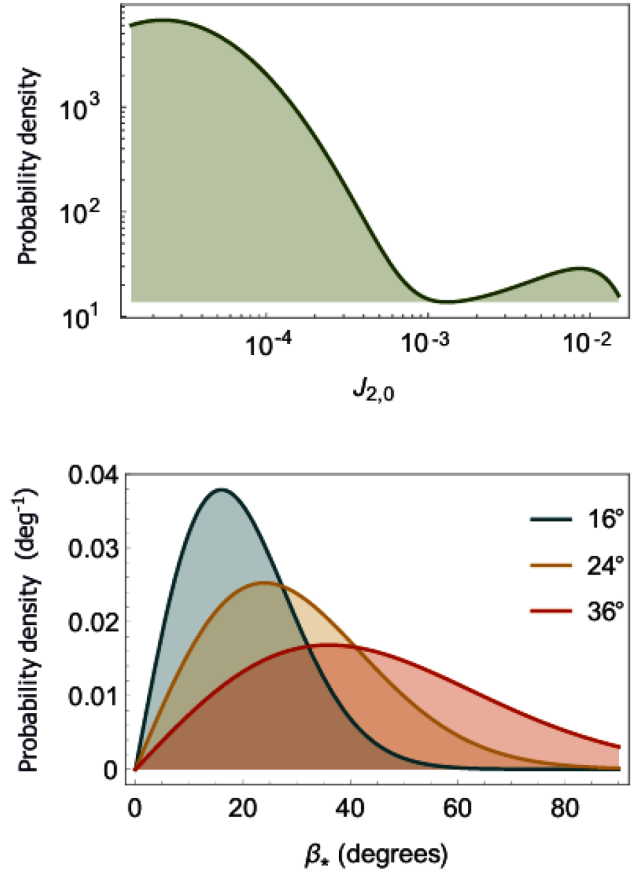
Figure 2. Probability densities of distributions from which $J_{2,0}$ and β_* were drawn when creating interpolation input sets. The curve in the upper panel is a fit to data collected by Karim et al. (2016) and Briceño et al. (2005) from T Tauri stars in the Orion OB1 association. These sample stars possess masses within the range [0.47, 1.09] Solar masses and radii within [0.88, 1.66]R_*. The Rayleigh curves in the lower panel were generated using scale parameters equal to 16 (mean stellar obliquity $20°$), 24 (mean $30°$), and 36 (mean $45°$).
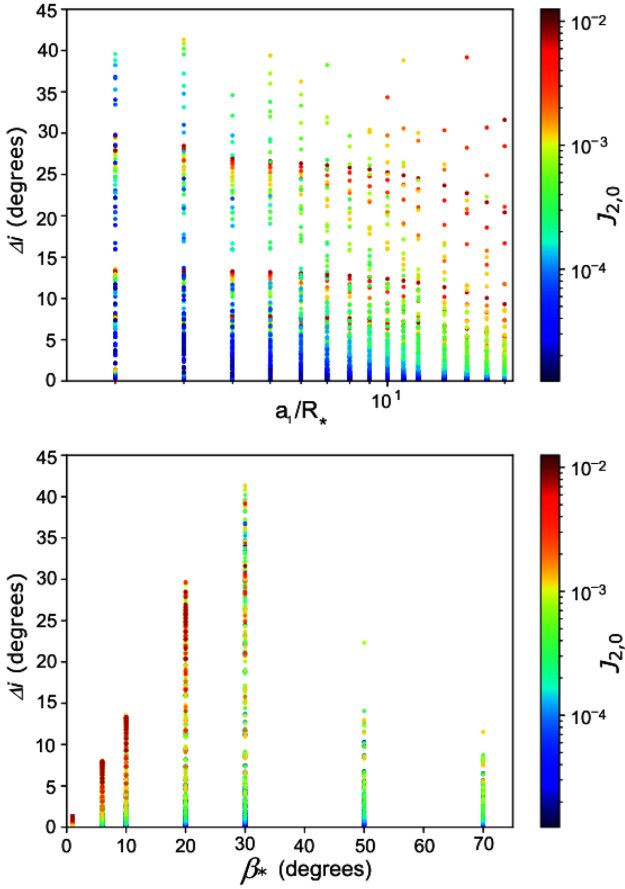
from this distribution. Note the bimodal shape, likely indicative of the dichotomy between disc-hosting and disc-free stars (Rebull et al. 2018). Disc-hosting stars are thought to have their spin rates locked to the disc, whereas disc-free stars are free to contract and spin-up (Armitage & Clarke 1996).

The true distribution of evolved and early stellar obliquities remains an area of active research, in which a number of possible distributions have been proposed (Fabrycky & Winn 2009; Winn et al. 2017). To investigate the influence of different obliquity distributions on mutual inclination signatures in the OTS context, we choose four distributions from which to draw inputs: three Rayleigh distributions with means of $20°$, $30°$, and $45°$ (see the bottom panel of Fig. 2), and one uniform distribution on [0, 90]°. Consequently, we generated four separates sets of 'artificial' Δi values, each based on randomly selected inputs from the three distributions of a_1, m, and $J_{2,0}$ and one of the β_* distributions.

3 RESULTS

Fig. 1 provides an example of the relationship between a stable planet pair's Δi evolution and the strength of the central host's quadrupole moment, for $20°$ stellar obliquity. In every case, the
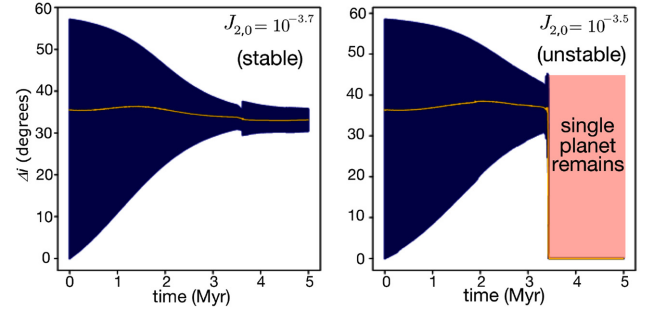
Figure 4. Mutual inclination evolution of two planet pairs of identical mass, position, and stellar obliquity. The left-hand panel was initiated with $J_{2,0} = 10^{-3.7} \approx 2 \times 10^{-4}$, while the right-hand panel was initiated with $J_{2,0} = 10^{-3.5} \approx 3.14 \times 10^{-4}$. As in Fig. 1, the gold curve represents average mutual inclination. Note that despite the relatively small increase in $J_{2,0}$, the right-hand system undergoes dynamical instability leaving an intrinsically-single system (red, shaded region).
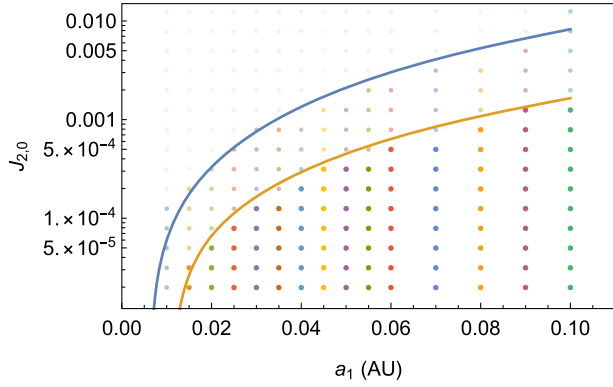
slightly higher, for the lowest mass systems over the highest mass systems. As mass-dependent separation seems to be a feature of *Kepler* systems (Weiss et al. 2018), we conclude that the OTS mechanism is largely independent of planetary mass in *Kepler*-like, subgiant planet pairs of equal mass.

It can be seen in both panels of Fig. 3 that, for a given β_*, larger $J_{2,0}$ leads to larger mean Δi, as expected. Interestingly, no planet pairs reach mean mutual inclinations exceeding about 40°. This is emphasized by the absence of a high-$J_{2,0}$ band in the 30° 'layer' of the upper panel, and the 30° column of the lower panel. This suggests that there exists a mean mutual inclination limit, between 35° and 40°, above which planet pairs go unstable. Such a limit has been suggested to result from the crossing of a high-inclination secular resonance (Spalding et al. 2018). Our results here suggest that instability is not necessarily triggered when the planet pair crosses a critical, instantaneous Δi, but rather when the time-averaged Δi grows high enough.

To illustrate this, Fig. 4 shows two alike systems' Δi evolution, where one remained stable and the other did not. The doomed system goes unstable at approximately 36° Δi (3.3Myr), but not at the first instance of that value, and not at mutual inclinations larger than that value. The stable system peaks at the same value of Δi, but does not demonstrate any signs of irregular excitation until much later in its evolution (about 3.6 Myr, 34° Δi), after which it continues to evolve smoothly. Thus, the requirement for instability remains poorly constrained in a theoretical sense, but appears more closely tied to the system's average state than to its instantaneous state.

Our results allow us to more generally separate initial stellar conditions into those that favour stability and those that are hostile to it. In the bottom panel of Fig. 3, for example, it is clear that planet pairs begin to go unstable for some obliquity between 20° and 30°. Moreover a larger fraction go unstable at 50° than 30°, suggesting that the critical $J_{2,0}$ required for instability is dependent upon the stellar obliquity. It was previously estimated that the critical $J_{2,0}$ separating stable from unstable dynamics lies close to 10^{-3} (Spalding et al. 2018); however, our results allow us to place more general constraints upon this requirement.

The critical $J_{2,0}$ required to initiate instability is illustrated in Fig. 5. All of the surviving systems from each of the three ranges of obliquity (0°–20°, 30°, and 50°–70°) are plotted according to $J_{2,0}$ and a_1. The points representing each range are plotted with increasing opacity, such that 0°–20° points are the faintest and 50°–70° the most

Figure 3. Main integration results. Dot colour in both panels corresponds to the value of $J_{2,0}$ at which the represented system was initialized. Upper panel: Final mutual inclination between planets, as a function of separation between host star and innermost planet. One can consider this plot as being comprised of multiple layers of data, each associated with a different initial value of β_*. Dark red, high-oblateness bands appear at the maximum attainable values of Δi in each layer. The most prominent bands at 14° and 27° belong to the layers of data associated with 10° and 20° of stellar obliquity, respectively. Lower panel: final mutual inclination as a function of stellar obliquity.

mean Δi, represented by the gold curve, and maximum Δi come close to converging on a single value by the end of the simulation, which is expected when $J_2 \to 0$ and the two orbits precess around their total angular momentum vector. The system in the lower right-hand panel was initiated with an unusually strong stellar quadrupole moment ($J_{2,0} \sim 8 \times 10^{-3}$). During the first million years of this simulation, the mutual inclination oscillates between $\sim 0°$ and $2\beta_* = 40°$, as expected in a system with a large, time-independent J_2 (see equation 16 of Spalding & Batygin 2016). However, in the case considered here where J_2 decays with time, the maximum Δi also falls with time, reaching roughly $1.5\beta_*$ by the end of the simulation. Thus, stellar spin-down alone tends to slightly reduce mutual planet-planet inclinations when compared to their maximum, constant-spin value.

The mean final mutual inclinations of systems that remained intact at the end of integration are plotted in both panels of Fig. 3. Note that mass is not a featured parameter in this figure, although it was a core variable in our initial inquiry. We found that any variation in planet mass within the range we adhered to was offset by the mass dependence of planet–planet separation (see equation 4). Mutual inclinations were only marginally larger, and instability rates only

Figure 5. The $m = 5$-$M_\oplus$ subset of numerically integrated systems, plotted as initial oblateness versus innermost semimajor axis. More opaque points correspond to larger initial stellar obliquities. The blue curve marks the approximate values of $J_{2,0}$ above which a system with $30°$ stellar obliquity will eventually go unstable. The orange curve denotes the same boundary for obliquities at or above about $50°$ (see equation 10).

visible. Points are not plotted in each case where instability occurred. Empirical fits to the stability limit for $30°$ and $50°$ have been overlaid, in order to approximate the boundary between stable and unstable $J_{2,0}$ using an analytic function. The two curves of critical J_2 are represented by the functions

$$J_{2,crit} = \begin{cases} -5 \times 10^{-5} + 0.003x + 0.8x^2 & \text{if } \beta_\star = 30° \\ -5 \times 10^{-5} + 0.003x + 0.14x^2, & \text{if } \beta_\star \geq 50° \end{cases} \quad (10)$$

where x corresponds to the innermost semimajor axis a_1, in AU. The similarity between the above expressions to leading order in x suggests that, by tuning the coefficient of the quadratic term, one can predict the approximate value of $J_{2,0}$ at which a close-in, similar-mass planet pair will go unstable for any stellar obliquity between $30°$ and $70°$. As our investigation did not include obliquities between $20°$ and $30°$, or above $70°$, we cannot extrapolate our instability predictions into these spaces. Nevertheless, with this data set, we have placed more precise constraints on the stellar properties required to eventually trigger instability in a given *Kepler*-like planet pair.

The critical mutual inclination angle for instability here is similar to the critical inclination of $\sim 39°$ required to enter the Kozai–Lidov resonance, in the case of a single planet perturbed by an exterior companion (Kozai 1962). This similarity was noted in Spalding et al. (2018), but the critical angle 2ω was not found to librate within resonance, counter to the case expected for the Kozai–Lidov resonance. Nevertheless, it remains intriguing that instability under the OTS mechanism shares traits with Kozai–Lidov resonance. The Kozai–Lidov mechanism has been studied mainly in systems where the perturbing and perturbed objects possess unlike masses and are widely separated (Naoz et al. 2011; Naoz 2016); it is unclear how the mechanism translates to systems comprised of closely spaced, Earth-sized planets like those modelled here. Such an analysis is beyond the scope of this work.

A more surprising result of our simulations emerges upon examining the properties of systems after undergoing instability. Specifically, after instability, only a single planet survives. Naively, it might be expected that a single planet that results from instability should exhibit a larger spin-orbit misalignment than a system that remained stable. Fig. 6 presents the orbital inclination evolution of every single planet in the $\beta_\star = 30°$ group that remained after instability, losing its partner in the process. Orbital inclination takes on the traditional Keplerian definition here and, in a single-planet
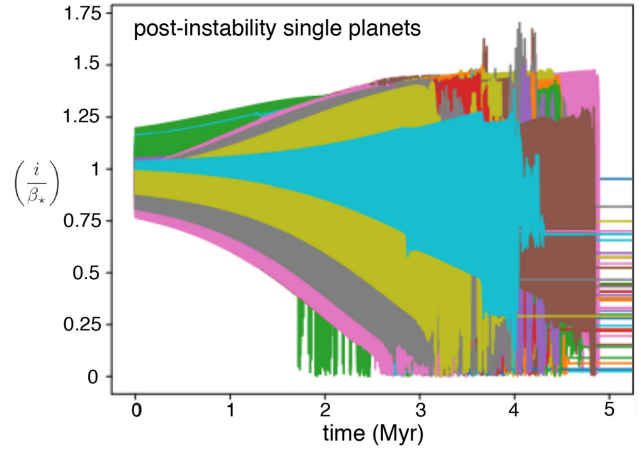

Figure 6. Orbital inclination evolution of all singles that survived instability while in orbit around an initially $30°$-tilted star. Inclination has been scaled by stellar obliquity (see Fig. 7) The survivors' final scaled inclinations have been extrapolated beyond the simulation's 5Myr runtime to more clearly show their final values.
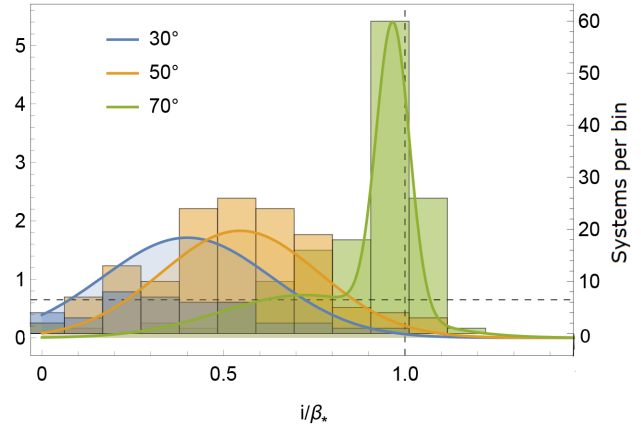
Figure 7. Raw data (histograms) and probability distributions of lone surviving planets' final orbital inclinations. Each inclination has been scaled, grouped, and colored according to the host's initial stellar obliquity. The horizontal dotted line approximates the form these distributions would take if they were entirely uniform (i.e. if post-instability orbital inclinations were entirely random).

system, is geometrically equivalent to stellar obliquity. The survivor's final orbital inclination is expressed as a fraction of the host's initial obliquity. Crucially, the surviving planet's final orbit was more aligned with the host's equatorial plane than it was at the beginning of the simulation.

The efficacy with which instability reduces stellar obliquity is further illustrated in Fig. 7. Here, scaled orbital inclinations of all survivors in the entire data set, grouped by initial stellar obliquity, are plotted in a histogram, along with probability densities for each group. These densities resemble normal distributions, with clear peaks and symmetry in the $30°$ and $50°$ cases. Moreover, the mean ratio of final orbital inclination to initial stellar obliquity increases with $\beta_\star$, with a sudden shift in concentration and peak placement between the $50°$ and $70°$ populations. That is, when a system with only moderate misalignment between host and planetary orbits goes unstable, the new stellar obliquity is fairly similar to its original value.
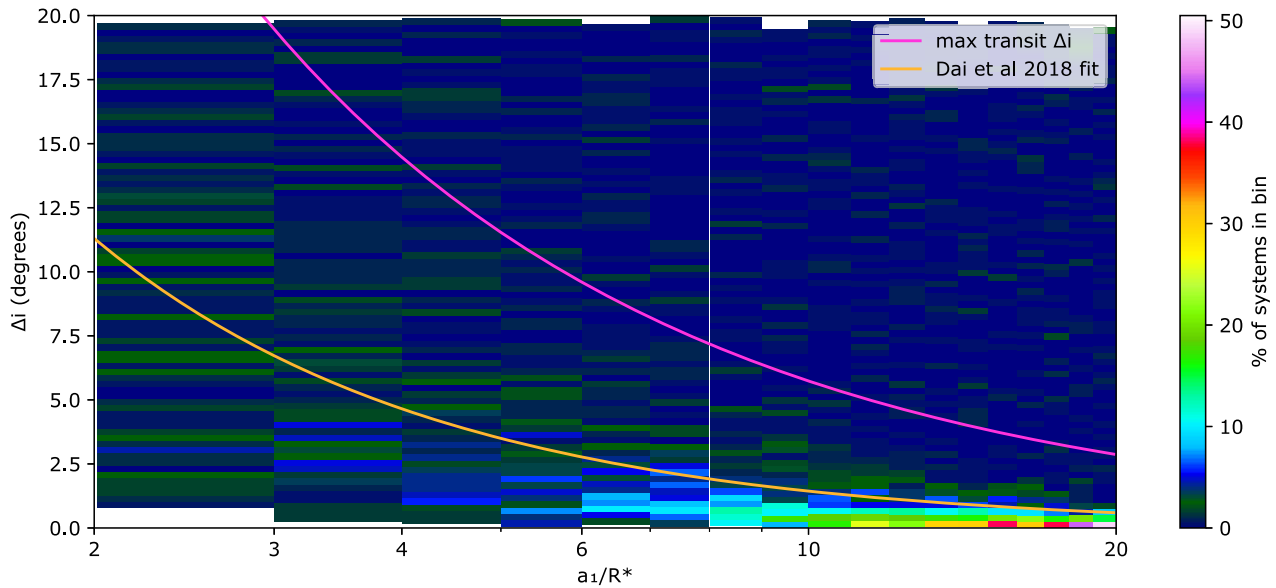
Figure 8. A 2D histogram of interpolated Δi data based on our integration results, where the input $\beta_\star$ set is Rayleigh-distributed with a mean of $20°$. Every column is a self-contained density plot: The colour of a given bin expresses the number of systems in that bin as a percentage of the total number of systems in the column containing that bin. The overlaid curve in magenta marks the boundary between mutual inclinations that permit both planets to be observable via the transit method, and mutual inclinations that essentially restrict the pair to a single-transiting configuration. The orange curve is the function found by Dai et al. (2018) to best fit their observed mutual inclination data, converted from a series of distribution widths to a series of mean mutual inclinations for ease of comparison.

This is in contrast with initially strongly misaligned systems, which experience more extreme obliquity erasure as a result of instability.

We elaborate upon this peculiar feature of our results later, but for now we suggest that stellar obliquity may not necessarily be expected to act as a signpost of dynamical instability. Rather, the process of instability tends to reduce stellar obliquities relative to systems where the two planetary orbits become misaligned, yet remain stable.

3.1 Mutual inclinations versus orbital distance

The mutual inclination of planet-pairs appears to increase close to the host star (Dai et al. 2018), a pattern that is consistent with the OTS mechanism (Li et al. 2020). In this section, we replicate this result using our modeled population as outlined in Section 2.3. We randomly sample from the uniform distributions of a_1 and m, and from the distributions of $J_{2,0}$ and $\beta_\star$ illustrated in Fig. 2, choosing $20°$ as the most common stellar obliquity (Winn et al. 2017). We then input these four sampled values into an interpolation of our simulated data to produce an artificial mutual inclination value. In total, 5000 artificial Δi were generated this way and are plotted in Fig. 8. The best-fitting observed relationship found by Dai et al. (2018) is overlaid in orange for comparison.

We note that the projected mutual inclinations between orbits as inferred in e.g. Dai et al. (2018) serve as lower limits to the true mutual inclinations. This is true for two reasons. First, by requiring that the planets mutually transit, the inferred mutual inclinations are bounded above by $\sim R_\star/a$. Secondly, the orientations of the orbits with respect to the viewer affects the orientations and relative lengths of the transit chords. In the simplest case of two circular but mutually inclined orbits, the mutual inclination as inferred from transit chord lengths is modulated by $\sim \sin(\theta)$, where θ is related to the viewing direction. If $\theta = 0$, the intersection of the orbits is along the viewing direction and both chords are the same length. The average value of

$\sin(\theta)$ from $0 < \theta < \pi$ is $2/\pi$, and so in an approximate sense, our simulations overestimate the mutual inclinations by $\pi/2$. We ignore this effect given that $2/\pi$ is of order unity.

A qualitative inspection of Fig. 8 confirms that, when operated upon by the OTS mechanism, the closest-in planet pairs experience the greatest level of mutual inclination excitation. This result was arrived at using stellar properties drawn from observationally motivated distributions, and thus arises naturally from the typical parameters characterizing planet-hosting stars. If the OTS mechanism is the main driver of excitation, the trend seen by Dai et al. (2018), and linked to the stellar quadrupole theoretically by Li et al. (2020), will continue to strengthen as more close-in mutual inclinations are constrained.

Interestingly, our choice of the mean $\beta_\star$ had minimal influence over the appearance of Fig. 8. Thus, we cannot place significant constraints upon the true distribution of early stellar obliquities from these results alone. On the other hand, stellar obliquities of $\sim 20°$ are well within observational constraints (Winn et al. 2017), hinting at a critical role played by the OTS mechanism in sculpting the final distribution of mutual inclinations.

4 DISCUSSION

All planetary systems begin their lives within a protoplanetary disc encircling a rapidly-rotating, inflated host star. While the gas disc is present, the planetary orbits are generally forced into coplanarity (Kley & Nelson 2012). However, for ~ 100 Myr subsequent to disc-dispersal, the host star remains rapidly rotating (Bouvier et al. 2014; Amard et al. 2016). If the host star possesses a non-zero obliquity, it is often capable of disrupting the primordial coplanarity of close-in systems. In contrast to these early stages of planetary system evolution, most planets are observed at ages exceeding a Gyr (Johnson et al. 2017; Petigura et al. 2017). By this time, their host

stars have typically spun down to periods exceeding a week, leading to a highly reduced J_2.

For the shortest period systems, the modern-day J_2 can still be dynamically significant (Becker et al. 2020; Li et al. 2020), particularly for so-called USPs, with periods shorter than 1 d (corresponding to $a \lesssim 0.02\,\mathrm{AU} = 4\,\mathrm{R}_\odot$). Nevertheless, these systems, too, must have passed through an earlier epoch of enhanced J_2, followed by decay of the J_2. Throughout this process, the dynamical system will inevitably sweep multiple secular resonances (Ward 1981) and potentially undergo instabilities (Spalding et al. 2018). Thus, it is important to determine the population-scale observational features expected to result from this ubiquitous process of stellar spin-down.

In this work, we simulated a population of planetary systems subject to the dynamical influence of their host stars' quadrupole moment, taking account of the subsequent decay of their J_2 over time. Among systems that remained stable, shorter innermost orbital periods are associated with greater mutual inclinations (see Fig. 8). This result was arrived at previously by Li et al. (2020), and agrees with observational work (Dai et al. 2018). However, our work indicates that when stellar obliquity exceeds $\sim 30°$, large J_2 has the potential to drive dynamical instability. Moreover, we compute the the critical J_2 required to cause instability for various stellar obliquities (Fig. 5).

Similarly to the excitation of mutual inclinations, close-in systems are more susceptible to instabilities (see Fig. 5). This is consistent with a picture, described in Spalding et al. (2018), wherein the stellar quadrupole drives mutual inclinations sufficiently high to access high-inclination secular resonances. It is passage through these resonances that eventually de-stabilizes the planetary system, a topic to which we now turn.

4.1 Instability and a mixed population

The original puzzle of the 'Kepler Dichotomy' was that too many single-transiting systems exist to arise from a homogenous population of mutually inclined multiplanet systems (Johansen et al. 2012; Ballard & Johnson 2016; He et al. 2019). In general, this mystery can be solved by either a separate population of systems that intrinsically host only a single planet, or alternatively, by an additional population of multiplanet systems possessing larger typical mutual inclinations. Between these options, the latter is typically favoured by observations (Zhu et al. 2018; He et al. 2019). Moreover, the shortest period planets that are most susceptible to the stellar quadrupole (the USPs) are inferred to host exterior companions most of the time (Sanchis-Ojeda et al. 2014; Adams et al. 2020). Nevertheless, these studies have so far not ruled out that ~ 10 per cent of the signal from single-transiting planets may arise from intrinsically-single systems. Rather, a poorly constrained, if subdominant fraction may be intrinsically single.

In this work, using reasonable estimates for the planetary architectures and stellar parameters, we found that a substantial fraction of initially coplanar systems may undergo instability as a response to the OTS. Such instability was previously revealed to act for a small number of specific systems (Spalding et al. 2018), and generally occurred only for stellar obliquities exceeding $\sim 30°$ and $J_2 \gtrsim 10^{-3}$. In this work, we likewise find that the onset of instability occurs near $30°$ of obliquity, but the precise tilt depends upon the system's J_2 and semimajor axis (see Fig. 5). Across the entire parameter range, the value of J_2 required to destabilize a system varies by a factor of five.

In order to get a sense of the potential prevalence of instability from the OTS mechanism, suppose for definiteness that systems possessing both $\beta_\star > 30°$ and $J_{2,0} > 10^{-3}$ undergo instability. If stellar obliquities follow a Rayleigh distribution peaked at $20°$
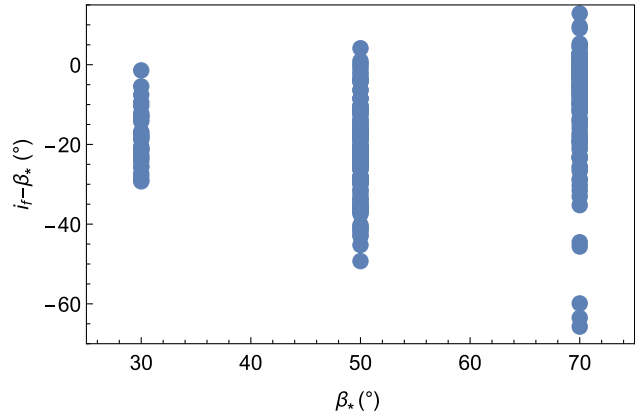
Figure 9. All surviving single-planet systems from our simulation, plotted according to the total orbital inclination shift (final minus initial) each single experienced as a result of instability. Negative values indicate relaxation from a high-inclination orbit on to a lower-inclination orbit, which is equivalent to a reduction in stellar obliquity.

(Winn et al. 2017), then about 32 per cent of stars would be tilted beyond $30°$. In tandem, about 39 per cent of stars used to construct the upper panel of Fig. 2 possess $J_{2,0} > 10^{-3}$. Assuming that $\beta_\star$ and $J_{2,0}$ are statistically independent, these occurrences imply that about 13 per cent of systems like those studied here are susceptible to instability through the action of the stellar quadrupole potential. This number is only included as an estimate, given the uncertainties associated with stellar obliquities and initial spin rates.

Moreover, a plethora of alternative pathways toward instability are available for close-in planetary systems (Chambers, Wetherill & Boss 1996; Ford & Rasio 2008; Batygin, Brown & Betts 2011; Johansen et al. 2012; Petit et al. 2020; Pichierri & Morbidelli 2020; Tamayo et al. 2020). Generally speaking, over ~ 10 per cent of systems within the context of our simulations are expected to end up as true single planets. This fraction of intrinsic singles has been difficult to rule out in previous surveys (Sanchis-Ojeda et al. 2014) and has been favored by the forward modelling approach of He et al. (2020). A promising avenue toward observational tests is to compare the obliquity distributions of single and multitransiting systems using the line-of-sight rotational velocity of the host star (Morton & Winn 2014; Winn et al. 2017).

Usually, it may be assumed that the singles will exhibit augmented spin-orbit misalignments if they arose from dynamical instability. However, our results suggest that when stellar oblateness drives instability, the one remaining transiting planet tends to possess a smaller spin-orbit misalignment than it did when it was younger (see Figs 7 and 9). In other words, suppose that a population of primordially multiplanet systems emerge from the disc with a distribution of stellar obliquities $\beta_\star > 30°$. If all of these systems are driven to instability, then the mean stellar obliquity of the resulting transiting singles is smaller than that of the primordial population, including many examples with $\beta_\star < 30°$.

Observationally, these systems would appear to exhibit a low stellar obliquity, while providing no evidence of additional close-in planets. A possible hallmark of such 'violently aligned' systems would be high eccentricity, despite low inclination, such as K2-25b (Gaidos et al. 2020; Stefansson et al. 2020). Moreover, eccentricities of single-transiting planets appear higher than those of multis (Xie et al. 2016; Van Eylen et al. 2019), which indicates a violent history. It should be noted, however, that the remaining single is rarely

brought to within $\sim 10°$ of the stellar equator, so would usually still arrive at its final orbit with a non-zero spin-orbit misalignment. Moreover, a central difficulty with using eccentricity as a tracer is that tides are expected to efficiently damp eccentricities in most systems residing close enough for the stellar quadrupole to be effective. Thus, eccentricity can only be used as a tracer of instability for a subset of single-transiting systems with longer tidal circularization times.

Broadening the scope beyond stellar oblateness-driven instability, we hypothesize that instability due to a misaligned external planetary perturber may result in an analogous degree of realignment between perturber and the planets surviving instability (Hansen 2017; Lai & Pu 2017). Future efforts are required to further delineate the mechanics of post-stability realignment.

4.2 Migration

Though we considered the time-evolution of the stellar J_2, we did not allow for migration among the planetary orbits. This is important because the orbits of USPs, analogue to the closest-in planets in our simulations ($\sim 0.01–0.02$ AU), are closer to the star than the hypothesized inner edge of protoplanetary discs (~ 0.05 AU; Armitage & Clarke 1996; Dullemond & Monnier 2010). Moreover, the high temperatures existing interior to the disc typically lie above the sublimation limit for silicates (Flock et al. 2019), preventing planet formation. Accordingly, lacking a local source of gas or dust, USPs are thought not to have formed *in situ* but rather to have migrated inwards subsequent to disc-dispersal (Lee & Chiang 2017; Winn et al. 2018; Petrovich, Deibert & Wu 2019; Millholland & Spalding 2020).

If USPs migrate within the first ~ 100 Myr after disc-dispersal, they will likely experience the large values of J_2 assumed here. However, if migration occurs later, then the planets currently residing within ~ 5 stellar radii will have never been subjected to the enhanced J_2 of a star at their current a_1, but at a larger, primordial value of a_1. This would likely reduce instability rates and final mutual inclinations, with the result that far fewer of the close-in systems in Fig. 8 could achieve the large mutual inclinations observed by Dai et al. (2018). It is unclear whether the time-scale on which inward tidal migration occurs is comparable to that of the weakening quadrupole moment.

In order to get a rough idea of when the J_2 is no longer sufficient, let us suppose that the perturbation of the inner planet from the outer member forces a nodal regression rate of (Murray & Dermott 1999)

$$\nu_{pp} \approx -\frac{3m_2}{4M_\star}\left(\frac{a_1}{a_2}\right)^3 n_1. \tag{11}$$

The equation above is only correct to a factor of ~ 2 as we have assumed that $a_1 \ll a_2$. However, for the purposes of the following calculation, no greater precision is required. In addition, the stellar oblateness forces a frequency of

$$\nu_\star \approx -\frac{3}{2}J_2\left(\frac{R_\star}{a_1}\right)^2 n_1. \tag{12}$$

If we use equation (8), we may write the ratio of these two frequencies in terms of the stellar spin period, such that

$$\frac{\nu_\star}{\nu_{pp}} \equiv \xi \approx \frac{8\pi^2}{3}k_2\frac{a_2^3}{Gm_2}\left(\frac{R_\star}{a_1}\right)^5\frac{1}{P_\star^2}$$
$$\sim 100\left(\frac{a_2}{0.06\,\text{AU}}\right)^3\left(\frac{m_2}{6\,\text{M}_\oplus}\right)^{-1}\left(\frac{P_\star}{\text{d}}\right)^{-2}\left(\frac{a_1}{5R_\star}\right)^{-5}. \tag{13}$$

If the USP is migrating inwards over a time-scale τ_a (such that $a_1 \propto \exp(-t/\tau_a)$), but the star spins down over a time-scale τ_s (such

that $P_\star \propto \exp(-t/\tau_s)$), and we assume that $R_\star$ is fixed, then the ratio above evolves according to

$$\xi(t) \approx \xi_0 \exp\left[-t\left(\frac{2}{\tau_s} - \frac{5}{\tau_a}\right)\right], \tag{14}$$

where $\xi_0 \sim 100$, depending upon a_2 and m_2. Computing $\mathrm{d}\xi/\mathrm{d}t$, we obtain

$$\frac{1}{\xi}\frac{\mathrm{d}\xi}{\mathrm{d}t} = \frac{5\tau_s - 2\tau_a}{\tau_a\tau_s}, \tag{15}$$

which is positive (i.e. the star's influence increases with time) if $2\tau_a < 5\tau_s$. In this case, the inner planet migrates inward rapidly enough to reach close proximity to the star before the quadrupole decays. In contrast, if $2\tau_a > 5\tau_s$, the stellar quadrupole diminishes as the planet migrates inward, weakening the influence of the stellar oblateness (see also Becker et al. 2020).

The simple arguments above should be expanded upon in future work. Nevertheless, we see that the critical aspect of incorporating migration into the oblate tilted star framework lies in the relative time-scales of migration and stellar spin-down. Both of these time-scales are poorly constrained during the earliest 100 Myr of the system's evolution (Bouvier et al. 2014; Spalding 2019).

Initially, the spin-down time-scales of Sun-like stars may range within 10–100 Myr (Garraffo et al. 2018; Spalding 2019). However, over longer time-scales, stars across a range of spectral types converge on to the so-called 'Skumanich' curve of $P_\star \propto t^{1/2}$ (Skumanich 1972; Garraffo et al. 2018), with the spin-down time-scale eventually reaching Gyr. The migration time of USPs remains an open question (Lee & Chiang 2017; Winn et al. 2018; Petrovich et al. 2019; Pu & Lai 2019), but it remains feasible that they migrate within the first 100 Myr, thereby experiencing an early period with an enhanced stellar quadrupole.

4.3 Initial conditions

All of our simulations assumed that the planetary orbits began in a coplanar arrangement, but possessed a non-zero inclination relative to the stellar equator. This assumption is equivalent to declaring that the disc disperses instantaneously, thus preserving any primordial star–disc misalignment in the form of planet–star misalignment (Spalding & Batygin 2016). However, in reality, disc-dispersal is a poorly understood process that may play out over time-scales ranging from centuries to hundreds of thousands of years (Alexander et al. 2014). If the disc disperses too slowly (that is, over several secular time-scales of about $\sim 10^3$ yr), the inner planets will simply realign adiabatically with the stellar spin axis, unless a sufficiently massive, exterior companion planet is present (Spalding & Millholland 2020).

Accordingly, our work here constitutes a thorough analysis of the consequences for planetary systems in the case where disc-dispersal occurs rapidly. In future work, it would be important to incorporate a range of disc-dispersal time-scales into our framework, including the interaction between the planets and the disc material itself. However, these additions are beyond the scope of the current work. For now, we note that the importance of the OTS mechanism, and indeed that of multiple other early dynamical processes, hinges upon the specifics of disc-dispersal.

Finally, we mention that whereas we assumed that J_2 monotonically decreases with time, in reality stars that lose their discs are often still contracting on to the main sequence. When the disc is present, magnetic star–disc torques are hypothesized to enforce disc-locking, preventing the contracting star from spinning up (Armitage & Clarke 1996; Rebull et al. 2018). Once the disc disperses, the

star continues to contract, but approximately conserves angular momentum, forcing it to spin-up. This involves both a reduction in stellar radius and an increase in spin period, both of which are essential factors in determining the strength of the star's quadrupole moment (see equation 8). If spin-up dominates physical contraction, we would see an initial upward trend in J_2, toward even larger values at the beginning of the post-disc phase. A J_2 spike could lead to more exaggerated final mutual inclinations and higher instability rates than are seen in our simulations. It is in the interest of future OTS inquiry that we question whether stellar contraction requires a change in the way we model time-dependent variation of the host's quadrupole moment.

We may estimate the influence that pre-main-sequence contraction has upon the stellar quadrupole moment using the following argument. First, we define the angular momentum of the host star as

$$\mathcal{J}_\star \equiv k M_\star \Omega_\star R_\star^2, \tag{16}$$

where k is the dimensionless moment of inertia (Sterne 1939). If $\mathcal{J}_\star$ is conserved ($d\mathcal{J}_\star = 0$), and we neglect the small changes in k and $M_\star$, we may relate the changes in $\Omega_\star$ to $R_\star$ with

$$2\frac{dR_\star}{R_\star} = -\frac{d\Omega_\star}{\Omega_\star}. \tag{17}$$

Next, using equations (8) and (12), we define the scaled quadrupole moment of the star as

$$\mathcal{L} \equiv J_2 R_\star^2 \approx \frac{1}{3} k_2 \frac{\Omega_\star^2}{GM_\star} R_\star^5. \tag{18}$$

As the star contracts, the evolution of the quadrupole moment is given by

$$\begin{aligned}
\frac{d\mathcal{L}}{\mathcal{L}} &= 2\frac{d\Omega_\star}{\Omega_\star} + 5\frac{dR_\star}{R_\star} \\
&= -4\frac{dR_\star}{R_\star} + 5\frac{dR_\star}{R_\star} \\
&= \frac{dR_\star}{R_\star} < 0, \tag{19}
\end{aligned}$$

where the second line has used relationship (17).

The simple calculation above indicates that, while the star is contracting immediately following disc-dispersal, its quadrupole moment also tends to decay, despite the increasing stellar rotation rate. Thus, our approximation of a monotonically-decreasing J_2 subsequent to disc-dispersal accurately reflects the true evolution of PMS stars.

We have not considered the evolution of k_2. In stars with $M_\star \gtrsim 0.3\,\mathrm{M_\odot}$, a radiative core forms during the PMS phase, which reduces the value of k_2 by up to an order of magnitude (Batygin & Adams 2013). However, this effect will also tend to decrease the quadrupolar potential. Cumulatively, the stellar quadrupolar potential is at its highest early-on, and decreases from there. Throughout this decay, the system crosses secular resonances that may lead to instabilities (Ward 1981; Spalding et al. 2018).

5 CONCLUSIONS

The large number of single-transiting planets within the *Kepler* data set, relative to multitransiting systems, continues to elude a full explanation. While the majority of these singles are likely to possess unseen inclined companion planets, an uncertain fraction may be truly single. In this work, we provided a population-level exploration of the hypothesis that the host star's quadrupole moment excites mutual inclinations within primordially coplanar, close-in

multiplanet systems. This oblate-tilted star (OTS) mechanism has previously been found effective in driving mutual inclinations among close-in planetary systems (Spalding & Batygin 2016; Li et al. 2020) and, if the star is tilted by more than ~30°, also acts as a ubiquitous pathway toward instability (Spalding et al. 2018). However, before this work, the OTS mechanism had not been subjected to a population-scale analysis.

In this paper, we drew from recent observations in order to construct a suite of *Kepler*-like planet pairs. Using empirically informed distributions of stellar obliquities and rotation periods, we simulated the orbital evolution of these systems in response to the host star's quadrupole moment immediately following disc-dispersal. Essential to the mechanism's effectiveness is the inclusion of early spin-down mechanics. Specifically, the stellar quadrupole decays due to spin-down and contraction of the star during the first ~100 million years, causing the secular effect of the oblateness to sweep over multiple secular resonances (Ward 1981). In contrast, a planet pair in orbit around a star with constant spin is unlikely to enter the secular resonance required to invoke instability (Spalding et al. 2018). Such a system will thus contribute only to the population of intrinsically two-planet systems.

Instability is the key to creating truly single planets in close orbits around their star. Broadly speaking, stellar spin periods below about 1–2 d (or $J_2 \sim 10^{-3}$), coupled with tilts exceeding ~30° are capable of driving instability (Fig. 5). Though stellar obliquities are poorly constrained for hosts of low-mass planets, up to 10 per cent of stars are expected to reside within this regime at some point during their histories. Accordingly the spin-down of the star and resulting incidence of instability must be considered when pursuing the question of the true nature of single-transiting planetary systems. We suggest that these singles are comprised of a mixture of lonely planets and those with excited, misaligned neighbors.

The exact proportion of apparent singles that are genuinely lonely depends on the rate at which stellar conditions – quadrupolar strength and obliquity – are favourable to large mutual inclination excitation and, ultimately, resonance. The 10 per cent instability rate we propose here is tentative, and will benefit from future investigations into early stellar misalignment and an improved understanding of the structure and rotation of young stars.

We have discovered a previously unreported phenomenon whereby the sole survivor of instability acquires a lower-inclination orbit than it possessed before the loss of its companion planet. That is, the spin-orbit misalignment of the one remaining planet is systematically lower than the spin-orbit misalignment of the initial two-planet system (Figs 7 and 9). This effect tends to reduce the observable stellar obliquity to roughly half of the initial angle. Therefore, despite the fact that larger initial misalignments cause instability, the phenomenon of obliquity reduction may damp the expected association between instability and large stellar obliquities (Morton & Winn 2014). As modern stellar obliquity measurements continue to be an area of interest (e.g. Winn et al. (2017) and Dai et al. (2020)), we predict that the projected distribution of observed stellar obliquities in single-transit systems will be similar to that of multitransit systems.

The outcome in a system undergoing evolution due to the OTS mechanism is sensitive to a number of early-stage factors that are not considered here. For example, this work did not include the brief interval of stellar spin-up that occurs while the star is still contracting on to the main sequence but the natal disc is removed. During this time, the cessation of star–disc torques facilitates a rapid decrease in rotational period and strength of quadrupolar moment. This 'spin-up' scenario widens the window in which inward-migrating planets can

be excited via the OTS mechanism, and has yet to be incorporated into numerical OTS investigations.

Further progress in the fields of disc dissipation, planet migration, young stellar modelling, and stellar obliquity evolution, particularly in understanding the relative time-scales of each, is also critical and will improve our ability to draw conclusions about this early and dynamically rich part of a planetary system's life cycle.

DATA AVAILABILITY

The data underlying this paper will be shared on reasonable request to the corresponding author.

REFERENCES

Adams E. R. et al., 2020, Planet. Sci. J. preprint (arXiv:2011.11698)
Akeson R. et al., 2013, PASP, 125, 989
Albrecht S. et al., 2012, ApJ, 757, 18
Alexander R., Pascucci I., Andrews S., Armitage P., Cieza L., 2014, Protostars and Planets VI. Univ. Arizona Press, Tuscon, AZ
Amard L., Palacios A., Charbonnel C., Gallet F., Bouvier J., 2016, A&A, 587, A105
Armitage P., Clarke C., 1996, MNRAS, 280, 458
Ballard S., Johnson J. A., 2016, ApJ, 816, 66
Batygin K., 2012, Nature, 491, 418
Batygin K., Adams F. C., 2013, ApJ, 778, 169
Batygin K., Brown M. E., Betts H., 2011, ApJ, 744, L3
Becker J. C., Adams F. C., 2016, MNRAS, 455, 2980
Becker J. C., Adams F. C., 2017, MNRAS, 468, 549
Becker J., Batygin K., Fabrycky D. C., Adams F. C., Li G., Vanderburg A., Rodriguez J. E., 2020, AJ, 160, 10
Bouvier J., Matt S. P., Mohanty S., Scholz A., Stassun K. G., Zanni C., 2014, Protostars and Planets VI. Univ. Arizona Press, Tucson, AZ
Briceño C., Calvet N., Hernández J., Vivas A. K., Hartmann L., Downes J. J., Berlind P., 2005, AJ, 129, 907
Bryan M. L., Knutson H. A., Lee E. J., Fulton B., Batygin K., Ngo H., Meshkat T., 2019, AJ, 157, 52
Chambers J. E., 1999, MNRAS, 304, 793
Chambers J., Wetherill G., Boss A., 1996, Icarus, 119, 261
Dai F., Masuda K., Winn J. N., 2018, ApJ, 864, L38
Dai F. et al., 2020, AJ, 160, 193
Davies C. L., 2019, MNRAS, 484, 1926
Dullemond C., Monnier J., 2010, ARA&A, 48, 205
Fabrycky D. C., Winn J. N., 2009, ApJ, 696, 1230
Fabrycky D. C. et al., 2014, ApJ, 790, 146
Flock M., Turner N. J., Mulders G. D., Hasegawa Y., Nelson R. P., Bitsch B., 2019, A&A, 630, A147
Ford E. B., Rasio F. A., 2008, ApJ, 686, 621
Gaidos E. et al., 2020, MNRAS, 498, L119
Garraffo C. et al., 2018, ApJ, 862, 90
Gladman B., 1993, Icarus, 106, 247
Gregory S. G., Adams F. C., Davies C. L., 2016, MNRAS, 457, 3836
Hansen B. M., 2017, MNRAS, 467, 1531
He M. Y., Ford E. B., Ragozzine D., 2019, MNRAS, 490, 4575
He M. Y., Ford E. B., Ragozzine D., Carrera D., 2020, AJ, 160, 276

Henrard J., 1982, Applications of Modern Dynamics to Celestial Mechanics and Astrodynamics. Springer, Dordrecht.
Johansen A., Davies M. B., Church R. P., Holmelin V., 2012, ApJ, 758, 39
Johnson J. A. et al., 2017, AJ, 154, 108
Kant I., 1755, General History of Nature and Theory of the Heavens. Petersen, Königsberg
Karim M. T. et al., 2016, AJ, 152, 198
Kley W., Nelson R., 2012, ARA&A, 50, 211
Kozai Y., 1962, AJ, 67, 591
Kraft R. P., 1967, ApJ, 150, 551
Lai D., Pu B., 2017, AJ, 153, 42
Lai D., Pu B., 2017, AJ, 153, 42
Laplace P. S., 1796, Exposition dy Système du Monde. Cerie-Social, Paris
Lee E. J., Chiang E., 2017, ApJ, 842, 40
Li G., Dai F., Becker J., 2020, ApJ, 890, L31
Lissauer J. J. et al., 2011, ApJS, 197, 8
Masuda K., Winn J. N., Kawahara H., 2020, AJ, 159, 38
Millholland S. C., Spalding C., 2020, ApJ, 905, 71
Millholland S., Wang S., Laughlin G., 2017, ApJ, 849, L33
Morbidelli A., 2002, Modern Celestial Mechanics: Aspects of Solar System Dynamics. Taylor & Francis, London
Morton T. D., Winn J. N., 2014, ApJ, 796, 47
Murray C. D., Dermott S. F., 1999, Solar System Dynamics. Cambridge Univ. Press, Cambridge
Naoz S., 2016, ARA&A, 54, 441
Naoz S., Farr W. M. Lithwick Y., Rasio F. A., Teyssandier J., 2011, Nature, 473, 187
Nobili A. M., Roxburgh I. W., 1986. in Kovalevsky J., Brumberg V. A., eds, IAUS 114, Cambridge Univ. Press, Cambridge, p. 105
Petigura E. A. et al., 2017, AJ, 154, 107
Petit A. C., Pichierri G., Davies M. B., Johansen A., 2020, A&A, 641, A176
Petrovich C., Deibert E., Wu Y., 2019, AJ, 157, 180
Pichierri G., Morbidelli A., 2020, MNRAS, 494, 4950
Pu B., Lai D., 2019, MNRAS, 488, 3568
Pu B., Lai D., 2020, preprint (arXiv:2008.05698)
Ragozzine D., Holman M. J., 2010, preprint (arXiv:1006.3727)
Rebull L., Stauffer J., Cody A., Hillenbrand L., David T., Pinsonneault M., 2018, AJ, 155, 196
Sanchis-Ojeda R., Rappaport S., Winn J. N., Kotson M. C., Levine A., El Mellah I., 2014, ApJ, 787, 47
Skumanich A., 1972, ApJ, 171, 565
Spalding C., 2019, ApJ, 879, 12
Spalding C., Batygin K., 2014, ApJ, 790, 42
Spalding C., Batygin K., 2016, ApJ, 830, 5
Spalding C., Millholland S. C., 2020, AJ, 160, 105
Spalding C., Marx N. W., Batygin K., 2018, AJ, 155, 167
Stefansson G. et al., 2020, AJ, 160, 28
Sterne T. E., 1939, MNRAS, 99, 451
Tamayo D. et al., 2020, Proc. Natl. Acad. Sci., 117, 18194
Van Eylen V. et al., 2019, AJ, 157, 61
Ward W. R., 1981, Icarus, 47, 234
Ward W. R., Colombo G., Franklin F., 1976, Icarus, 28, 441
Weiss L. M., Marcy G. W., 2014, ApJ, 783, L6
Weiss L. M. et al., 2018, AJ, 155, 48
Winn J. N., Fabrycky D. C., 2015, ARA&A, 53, 409
Winn J. N., Fabrycky D., Albrecht S., Johnson J. A., 2010, ApJ, 718, L145
Winn J. N. et al., 2017, AJ, 154, 270
Winn J. N., Sanchis-Ojeda R., Rappaport S., 2018, New Astron. Rev., 83, 37
Xie J.-W. et al., 2016, Proc. Natl. Acad. Sci., 113, 11431
Zhu W., Petrovich C., Wu Y., Dong S., Xie J., 2018, ApJ, 860, 101

This paper has been typeset from a TeX/LaTeX file prepared by the author.